Predicting the self-assembly of a model colloidal crystal

Daphne Klotsa[a] and Robert L. Jack[a]

Received Xth XXXXXXXXXX 20XX, Accepted Xth XXXXXXXXX 20XX

First published on the web Xth XXXXXXXXXX 200X

DOI: 10.1039/b000000x

We investigate the self-assembly (crystallisation) of particles with hard cores and isotropic, square-well interactions, using a Monte Carlo scheme to simulate overdamped Langevin dynamics. We measure correlation and response functions during the early stages of assembly, and we analyse the results using fluctuation-dissipation theorems, aiming to predict which systems will self-assemble successfully and which will get stuck in disordered states. The early-time correlation and response measurements are made before significant crystallisation has taken place, indicating that dynamical measurements are valuable in measuring a system's propensity for kinetic trapping.

1 Introduction

The self-assembly of individual components into ordered structures has been studied in a variety of contexts including biomaterials research[1,2] and nanoengineering[3–9]. Significant progress has been made in experimentally synthesising different building blocks designed to assemble into specific target products[10–12]. Assembling systems, however, often get stuck in metastable disordered states before reaching the equilibrium ordered ones. Kinetic traps are absent from classical theories of phase change[13] but they pose real problems in experiments such as those on protein and colloidal crystallisation[14–16]. In order to address the kinetics of self-assembly, out-of-equilibrium theories need to be developed.

Crystallisation is a well-studied process, whereby particles in a fluid state undergo a phase transition and develop long-ranged crystalline order. This spontaneous ordering is an example of self-assembly[17]. Controlling the crystallisation of proteins and colloids would have applications in biology (for example, in determining the structure of biomolecules[18]) as well as in photonics (for example, in controlling the propagation of light[19,20]). In both colloidal and certain biomolecular systems the constituent particles interact via an effective short-ranged attractive potential with repulsive 'hard' cores[21–27].

In this paper, we study crystallisation in a model colloidal system, as a simple example of self-assembly. A schematic phase diagram is shown in Fig. 1(a). We are concerned with the *dynamics* of the process whereby an initially homogeneous system phase separates into a crystal coexisting with a dilute fluid. The questions we address are the following: what happens during the process of assembly? How does a system that will eventually assemble into a crystal differ from one that will get kinetically trapped? What are the first signs of frustration

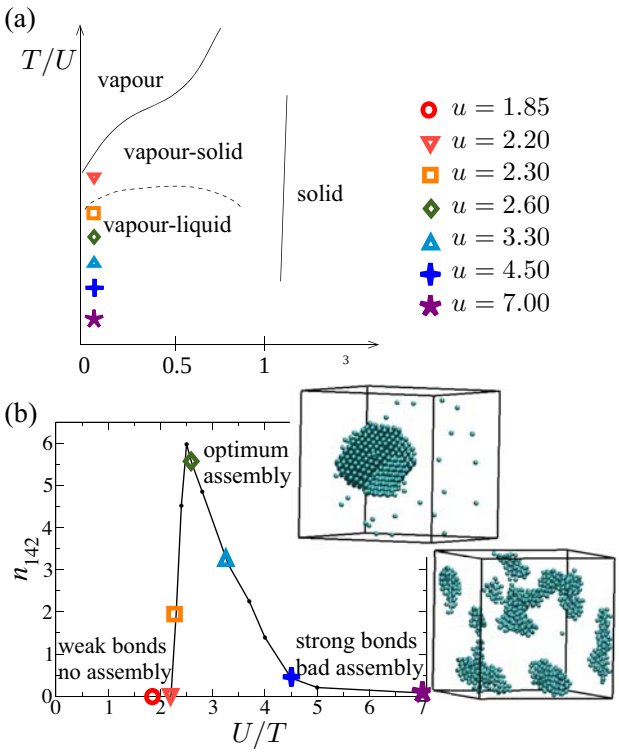

Fig. 1 (a) Schematic phase diagram for a square-well potential, following Ref.[28]. The legend shows the bond strengths ($u = U/T$) that will be considered in this work, with estimates of the locations of these state points within the schematic phase diagram. (b) We plot a measure of the crystallinity of the system, for various bond strengths, at a time $t = 10^6$ MC steps. The crystallinity is measured using a common neighbour analysis[29], as described in the main text. The colours of the symbols indicate the transition from high temperatures (red, weak bonds) towards low temperatures (violet, strong bonds).

[a] *Department of Physics, University of Bath, Bath BA2 7AY, United Kingdom. Fax: XX XXXX XXXX; Tel: XX XXXX XXXX; E-mail: r.jack@bath.ac.uk*

and when do they appear? How does the strength of attractive interactions influence the dynamics? What are the relevant physical quantities one should measure in order to understand the dynamics, and at what times should we measure them?

Self-assembly processes require a balance between a net drive to assembly and kinetic accessibility. The first requirement implies that the thermodynamic equilibrium state is an assembled one, which presupposes sufficiently strong attraction between individual components. The second requirement is kinetic and ensures that the thermodynamic state is accessible within reasonable timescales. The two requirements are competing, with the thermodynamic one favouring low temperatures and strong bonds and the kinetic one high temperatures and weaker bonds. Fig. 1(b) shows the crystallinity of the system as a function of the bond strength: its non-monotonic form demonstrates the competition between kinetic and thermodynamic effects, with a clear maximum at intermediate bond strengths.

In the past, the two competing requirements for effective self-assembly have been characterised through fluctuation-dissipation ratios (FDRs), which measure the extent to which equilibrium fluctuation-dissipation theorems (FDTs) continue to hold in out-of-equilibrium settings. In particular, it was shown[30] that correlation and response functions can provide a measure of the balance between the net drive to assembly and kinetic accessibility, and therefore indicate which systems will assemble into ordered structures and which ones will get kinetically trapped. Jack, Hagan and Chandler[30] investigated and compared two models: viral capsids and sticky disks. The purpose of this paper is to extend these ideas into a model colloidal system in order (i) to study whether the fate of this system can be predicted from the early stages of assembly based on FDR measurements, thus providing insight and subsequently guidelines for colloidal and protein crystallisation experiments and simulations; and (ii) to identify generic features of self-assembly that are not system-dependent.

Details of the computational model are given in section 2. In Section 3 we show how the system evolves in time for different interaction strengths, identifying regimes of slow nucleation, rapid assembly and kinetic trapping – features that are not predicted by the equilibrium phase diagram. We then introduce correlation and response functions in Section 4, explaining how they can be used to predict assembly quality. We include a discussion of the robustness of our measurements: how they depend on measurement times, interaction range and volume fraction. Finally, Section 5 gives a discussion of the results and poses questions for future investigation.

2 Model

We study a system of N spherical particles in a cubic box of volume V, with periodic boundary conditions. The particles have hard cores and isotropic, square-well interactions. Their hard-core diameter is σ, the depth of the potential is U and the range of interaction is $\xi\sigma$. Thus, the energy of the system is

$$E = -\frac{U}{2}\sum_i n_i \tag{1}$$

where n_i is the number of neighbours for particle i: that is, the number of particles within the interaction range $\xi\sigma$. It is also convenient to define $E_i = -\frac{1}{2}n_i U$.

As shown for example in Liu *et al.*[28], the short range of the attractions reduces the stability of the liquid phase, and the vapour-liquid binodal is metastable, lying within the vapour-solid coexistence curve. The phase diagram is sketched in Fig. 1(a). For simplicity we have defined $u = U/T$ which will be used to quote the bond strengths in the rest of the paper (we take Boltzmann's constant $k_\mathrm{B} = 1$ throughout).

Beginning with equilibrated systems of hard spheres, we used a Monte Carlo (MC) scheme as an approximate method to simulate the overdamped Langevin equation

$$\frac{\partial}{\partial t}\boldsymbol{r}_i = -\frac{D}{k_\mathrm{B}T}\nabla_i E + \boldsymbol{\eta}_i \tag{2}$$

where E is the total energy of the system, $\nabla_i = (\frac{\partial}{\partial x_i}, \frac{\partial}{\partial y_i}, \frac{\partial}{\partial z_i})$ as usual*, and the components of the vectors $\boldsymbol{\eta}_i$ are independent white noises.

On each move of our Monte Carlo scheme, we pick a random particle and propose a random displacement from a cube of side $2a_0$, centred at the origin. (Thus, the maximum displacement in each of the x, y and z directions is a_0.) We accept the move with probability $\min(1, \mathrm{e}^{-\Delta E/k_\mathrm{B}T})$ in accordance with detailed balance, where ΔE is the energy difference between the states before and after the proposed move. A Monte Carlo step (or sweep) consists of N Monte Carlo moves, and we associate it with a time increment τ_0. In the limit of $a_0, \tau_0 \to 0$ while holding $D = a_0^2/6\tau_0$ constant, this method provides dynamical trajectories in accordance with the Langevin equation (2) above†[31,32].

In the Langevin description, the natural unit of time is the Brownian time $\tau_\mathrm{B} = \sigma^2/D = (\sigma/a_0)^2\tau_0$. The behaviour of the model depends on the dimensionless parameters ξ and $u = U/T$ as well as on the particle volume fraction. Unless

* Strictly, $\nabla_i E$ is ill-defined, since E is not a continuous function of the particle coordinates. For the purposes of (2) we imagine regularising the square-well potential by taking a limiting case of a smooth but steep potential. In practice, we integrate this equation using a Monte Carlo scheme with a finite time step τ_0, which avoids the need for any explicit regularisation.

† An alternative to our MC scheme would be to use Brownian dynamics to simulate this system: in the limit of small time step τ_0 then both Brownian and MC dynamics are equivalent. One reason to prefer the MC in this study is that the fluctuation-dissipation theorems described in the following sections hold exactly for equilibrated systems with MC dynamics, even when the time step τ_0 is finite. (This is not the case when using Brownian dynamics.)

otherwise stated, our simulations are done at volume fraction 4% (i.e., $\pi N\sigma^3/6V = 0.04$), with N=1000 and ξ=0.11σ, and we take $a_0 = 0.15\sigma$. We quote times in MC steps (units of τ_0), noting that $\tau_B \approx 44\tau_0$ for our chosen step size a_0. We observe that this step size a_0 is comparable to the interaction range $\xi\sigma$, so that our results are not yet representative of the limit of small a_0. We have conducted simulations with smaller a_0: while quantitative differences are observed, qualitative features are unchanged. As usual, our time step (or equivalently, a_0) is chosen as a trade-off between accuracy of numerical integration and practical efficiency ‡.

3 Crystallisation process

In Fig. 2, we show results from dynamical simulations for various bond strengths u. In the stable fluid phase (e.g., $u = 1.85$), the system quickly relaxes into an equilibrium state where the average number of neighbours per particle

$$n(t) = \langle n_i(t) \rangle \tag{3}$$

is relatively small. Increasing the bond strength to $u = 2.3$, the system is in the fluid-solid phase coexistence region of the phase diagram, and nucleation is observed at a time $t \approx 6 \times 10^5$ MC steps. For stronger bonds, $u = 2.6$ and $u = 3.3$, the behaviour of $n(t)$ shows that the nucleation barrier is small so that clusters of particles grow smoothly, starting at early times. For very strong bonds $u \geq 4.5$, clusters of particles grow rapidly at early times, but this growth slows down at longer times. This is the kinetic trapping regime.

Recently, a lot of effort [21,27,35–41] has been devoted to the process of crystal nucleation, especially in the limit where the system is close to the binodal and nucleation is a rare event with an appreciable free energy barrier (this is also the limit where classical nucleation theory is applicable). In Fig. 2, the data at $u = 2.3$ lie within this regime, but it is clear that at optimal assembly conditions (for example $u = 2.6$) the free energy barrier for nucleation is quite small. In the absence of a large free energy barrier, methods such as umbrella sampling [35] and rare event sampling methods [38,41] are of limited use, since the process involves rapid formation of many clusters and a single reaction co-ordinate such as the size of the largest crystalline cluster does not describe the process effectively. Instead, we study the crystallisation process by direct simulation, without

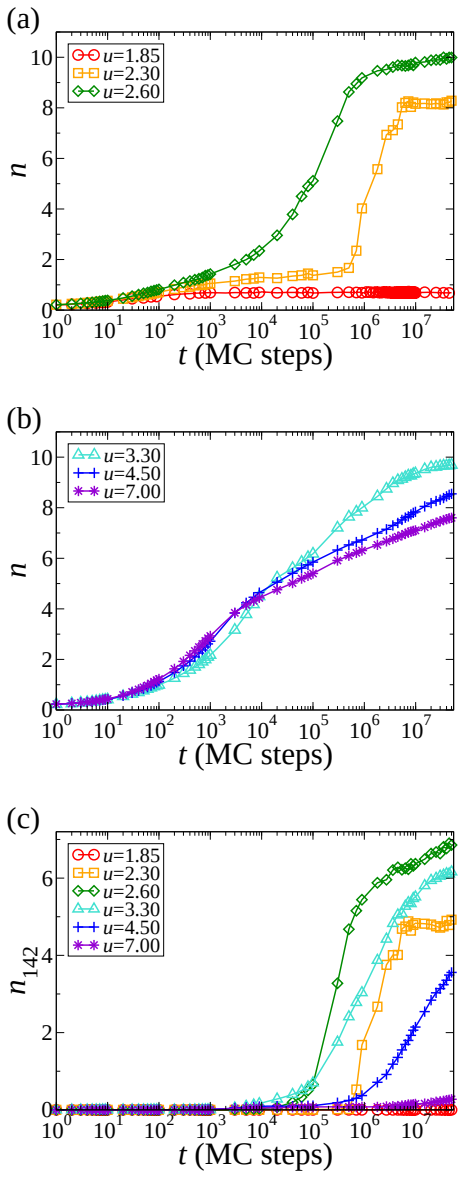

Fig. 2 (a,b) Average number of neighbours $n(t)$, plotted as a function of time, for different bond strengths. (c) The 'crystallinity' of the system as a function of time for the same six bond strengths. The definition of the order parameter $n_{142}(t)$ is discussed in the text. Each curve in this figure is an average over eight trajectories.

‡ In contrast to kinetic Monte Carlo simulations where the presence of an underlying lattice is assumed from the outset (for example, in surface science [33]), we work here in continuous space and take (2) as the fundamental description of our system. In models where the lattice structure is imposed, movement rates and acceptance probabilities in the MC scheme should be derived from interactions between the moving atoms and the existing crystal [33,34]. On the other hand, for systems described by (2), all physical quantities are fixed by the choice of the temperature T, the potential energy function E, and the diffusion constant D.

projection onto reaction co-ordinates or the assumption that the process is dominated by a single critical nucleus.

Another relevant question is whether crystallisation occurs directly from the homogeneous fluid, or whether amorphous ("metastable liquid") droplets form which then act as nucleation sites for the crystal[21,27,39–41]. Since crystal nucleation is not itself a rare event, there is little evidence for long-lived metastable states. However, for $u = 2.6$ and $u = 3.3$, we do observe the formation of amorphous clusters of particles at early times, with crystallisation occuring as these clusters bigger. For $u = 2.3$, we do not observe any long-lived - phous clusters – extrapolating from the results of Liu *et* we believe that this state is close to the metastable vapour binodal. These results are consistent with earlier servations[21,27] that nucleation is accelerated when the is unstable to liquid-vapour phase separation, in which nucleation occurs via the formation of large amorphous ters. For simulations at $u = 2.2$ (not shown) it is likely the fluid is unstable to crystallisation, but nucleation enough that it was not observed in direct simulations of 5×10^7 MC steps.

We use a common neighbour analysis (CNA)[29] to sure the crystallinity of the assembling system. In particular we count the number of bonded pairs of particles that 'crystallinity criterion'. The criterion is that pairs of particles have exactly four mutual neighbours, and those mutual bours must share exactly two bonds. We denote the number of bonded pairs that satisfy this criterion by N_{142}, and we - malise it by defining $n_{142}(t) = 2\langle N_{142}(t)\rangle/N$. This normalisation facilitates comparison with the number of neighbours $n(t)$ plotted in Figs. 2(a) and (b): if all bonded pairs in the tem satisfy our 'crystallinity criterion' then $n_{142}(t) = n$ the notation of Honeycutt and Andersen[29], we are measuring the combined number of 1421 and 1422 environments, which are indicative of cubic crystal structures. (In practical self-assembly processes, other structural features such as long-ranged crystalline ordering and the morphology and faceting of the crystal might also be important. However, for the general considerations of this article, we restrict our analysis to the CNA as a simple indicator of the yield of the assembly process.)

In Fig. 2(c) we show $n_{142}(t)$ for the same six indicative bond strengths considered so far. At early times n_{142} is small, with a sudden increase at later times, as crystallites form in the system. Taking the data from this figure at $t = 10^6$ MC sweeps, we obtain the 'yield' shown in Fig. 1. (Plotting the yield at later times shows similar results and is discussed in Section 4.3).

In Fig. 3(a), the number of bonds is plotted as a function of time for various temperatures, including the ones we have been focussing on up to now. The graph has been cropped so as to show the evolution of the system only up to 4000 time

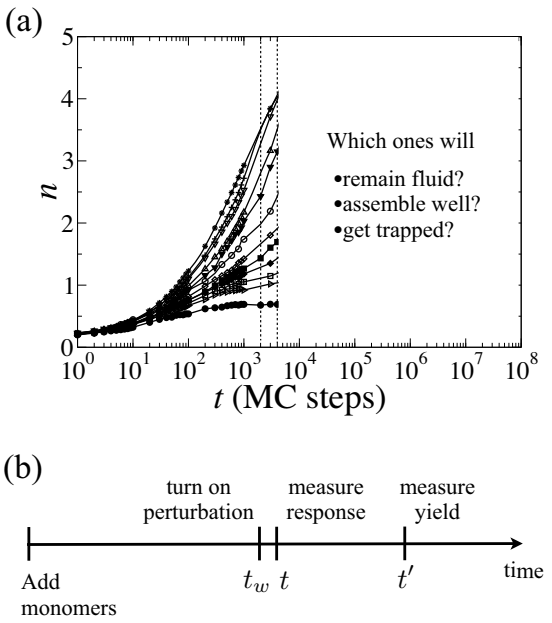

Fig. 3 (a) We plot $n(t)$ for various bond strengths, including the ones shown in Fig. 2, and showing only $t \leq 4000$ MC sweeps. From this information alone, we aim to predict the long-time fate of the system. (In fact, the three traces with largest n correspond to the strongest bonds, and will become kinetically trapped; the two with smallest n have weak bonds and will assemble poorly; away from the extremes there is a range of effective assembly, as shown in Fig. 2). The dashed lines define the narrow window over which the dynamical measurements will be made. (b) The simulation protocol used to measure the correlation and response functions, as described in the main text.

steps. We pose the following question: if we are not prepared to wait for the late-time information discussed earlier in this section, can we determine the fate of the system by looking at the dynamics so early on? In the remainder of the paper we demonstrate that the only information needed is, in fact, in the narrow window indicated by the dashed lines between 2000-4000 MC steps. We find that the long-term fate of the system is strongly correlated with certain early-time measurements that we now describe.

4 Predicting assembly quality

4.1 Reversible bonding, correlation and response functions

In predicting the long-time fate of the system, a central task is to identify the propensity of the system for kinetic trapping. Whitesides[42] observed that the reversible formation of weak bonds allows the system to escape from kinetic traps, facilitating good assembly, consistent with more recent studies[30,43,44]. Conversely, if attractive interactions between particles are too strong, then particles tend to aggregate into disordered clusters that grow rapidly and do not anneal into crystalline structures.

To distinguish these cases, we consider correlation and response functions that depend on the behaviour of the system between two times. Away from equilibrium, correlation and response measurements have been investigated in the theoretical study of glassy systems[45–47], in theories of non-equilibrium processes[48,49] as well as in self-assembling[30] and gelating systems[50]. Moreover, experimental developments have shown that measuring correlation-response functions may be a possible route for characterising dynamics in the lab too[51–53].

We define the (dimensionless) single-particle energy autocorrelation function as

$$C(t,t_w) = \frac{1}{U^2}\left[\langle E_i(t_w)E_i(t)\rangle - \langle E_i(t_w)\rangle\langle E_i(t)\rangle\right] = \tfrac{1}{4}\left[\langle n_i(t_w)n_i(t)\rangle - \langle n_i(t_w)\rangle\langle n_i(t)\rangle\right] \quad (4)$$

We adopt the convention that $t_w \leq t$, consistent with Fig. 3(b). For fixed t_w, the correlation function measures the extent to which the system's structure at t_w is correlated with its structure at some later time t. For example, in the equilibrium fluid state the $C(t,t_w)$ decays to zero on a time scale that reflects the lifetime of an interparticle bond.

Away from equilibrium, it is convenient to normalise this correlation function as

$$\tilde{C}(t,t_w) = \frac{C(t,t_w)}{C(t,t)} \quad (5)$$

The equal time correlation function $C(t,t)$ measures the variance in the number of bonds between particles, at time t. If

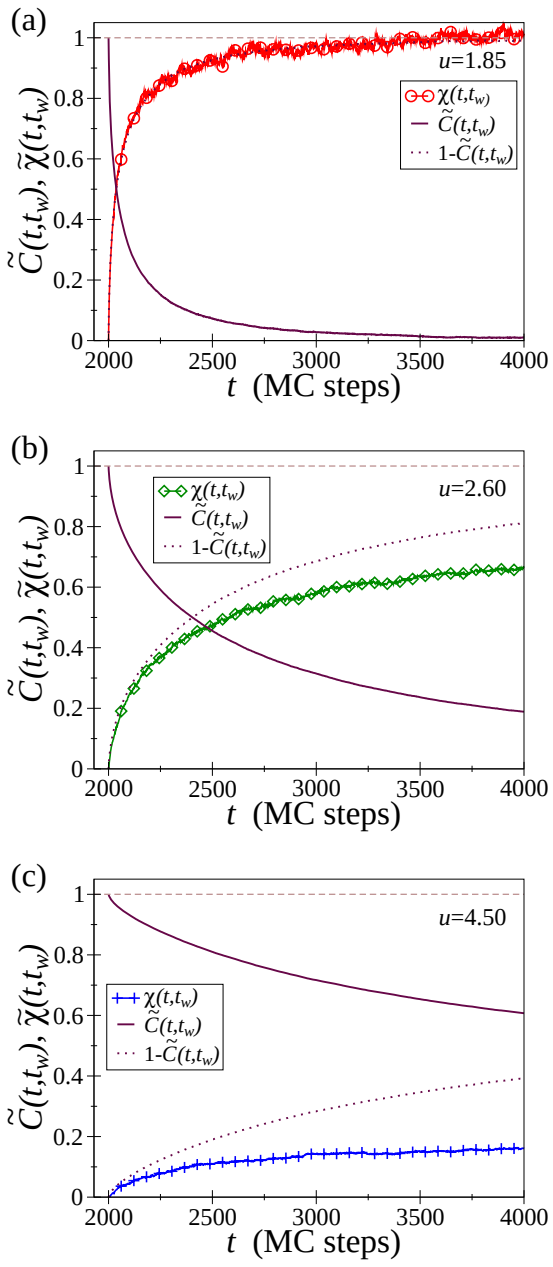

Fig. 4 Correlation $\tilde{C}(t,t_w)$ and response functions $\tilde{\chi}(t,t_w)$ are plotted versus time t for three different bond strengths. We also plot $1-\tilde{C}(t,t_w)$, for comparison with (8). (a) Bond strength u=1.85: the system is equilibrated in a dilute fluid phase. It is clear that $\tilde{\chi}(t,t_w) = 1-\tilde{C}(t,t_w)$, in accordance with FDT. (b,c) Bond strengths $u = 2.6$ and $u = 4.5$ respectively: both systems are far from equilibrium and the $\tilde{\chi}(t,t_w)$ differs strongly from $1-\tilde{C}(t,t_w)$. For the weaker bonds (panel b), the system will assemble into a crystal; for the stronger bonds (panel c), the system will become kinetically trapped.

bonding is irreversible (bonds never break), $\tilde{C}(t,t_{\rm w})$ may be interpreted as the fraction of bonds in the system at time t that had already been formed at the earlier time $t_{\rm w}$. Increasing t at constant $t_{\rm w}$, the system forms new bonds, and the correlation $\tilde{C}(t,t_{\rm w})$ decays towards zero. Thus, in contrast to the situation at equilibrium, the correlation function away from equilibrium does not simply measure a bond lifetime, but a combination of a bond lifetime and the rate of bond formation.

In order to separate these effects, we also consider a response function. The idea is that bond-making occurs whenever particles collide, so its rate is largely independent of the bond strength. On the other hand, bond-breaking processes require thermal activation over an energy barrier U and take place with rates proportional to $\mathrm{e}^{-U/k_{\rm B}T}$. On changing the strength of the forces between particles, the bond-breaking rate will change: measuring this response gives information about the relative likelihood of bond-making and bond-breaking in the system.

The protocol for measuring this response is shown in Fig 3(b). As before, we begin with an equilibrated system of hard spheres, and introduce the interaction potential U at time $t=0$. After a waiting time $t_{\rm w}$ we perturb the bond strengths in the system, so that the energy of the ith particle becomes $E_i=-\frac{1}{2}(U+\delta U_i)n_i$, where n_i is the number of neighbours of particle i (as above), while δU_i is the perturbation applied to the ith particle, and the factor of $\frac{1}{2}$ ensures no double counting of bonds. At a later time $t>t_w$, we measure the (dimensionless) response of particle i to the change in its bond strength:

$$\chi(t,t_{\rm w})=\frac{\partial\langle n_i(t)\rangle}{\partial(\delta U_i)}\frac{T}{2}. \qquad (6)$$

This response depends on $t_{\rm w}$ since the perturbation is applied only between times t and $t_{\rm w}$. In our simulations t and $t_{\rm w}$ vary within the window of 2000-4000 time steps as indicated by the dashed lines in Fig. 3(a).

As shown in Appendix A, $\chi(t,t_{\rm w})$ can be measured computationally by applying perturbations of magnitude δU_i to all particles, but with randomly chosen signs. The response is then obtained by comparing those particles with positive and negative values of δU_i. We take $|\delta U_i|=0.125U$ and have checked that for all bond strengths considered the perturbation is within the linear response regime.

In Appendix B, we prove the fluctuation-dissipation theorem (FDT) that links $C(t,t_{\rm w})$ and $\chi(t,t_{\rm w})$. Normalising the response as

$$\tilde{\chi}(t,t_{\rm w})=\frac{\chi(t,t_{\rm w})}{C(t,t)}, \qquad (7)$$

the FDT reads

$$\tilde{\chi}_{\rm eqm}(t,t_w)=1-\tilde{C}_{\rm eqm}(t,t_w) \qquad (8)$$

where we added the label 'eqm' to emphasise that this relation holds only at equilibrium.

Fig. 4(a) shows correlation and response functions that are typical for a system in the dilute fluid phase. The correlation function decays to zero as the system loses memory of its initial state, and the response grows in accordance with FDT, since the system is at equilibrium. Assembling systems, however, are far from equilibrium. Nevertheless, FDT can provide a useful comparison quantifying *how far* the systems deviate from "locally equilibrated" states[30]. From Fig. 2 it is evident that the system with $u=2.6$ will assemble into a crystal, within $\sim 10^6$ MC steps. In Fig. 4(b) we show correlation and response functions for the same system, at times long before crystal formation. It is clear that the response $\tilde{\chi}(t,t_{\rm w})$ is no longer equal to $1-\tilde{C}(t,t_{\rm w})$ (that is, FDT no longer applies). For the strongest bonds ($u=4.5$, Fig. 4(c)) the response is very small, indicating that bond-breaking events are rare, and therefore that disordered bonds are not annealed effectively: this will lead to kinetic trapping at later times (see Fig. 2).

4.2 Estimating fluctuation-dissipation ratios

In the context of glassy model systems, the clearest way to analyse correlation-response data is to fix the measurement time t and vary the time $t_{\rm w}$ at which the perturbation is applied[50,54,55]. (Note that this is not the case in Fig. 4 where correlation and response data are plotted as a function of t at fixed t_w.)

Correlation and response functions are plotted in this way in Fig. 5(a) and (b). For $t=t_{\rm w}$, the response vanishes since the perturbation has had no time to act; as $t_{\rm w}$ decreases towards zero, there is an increase in the time $t-t_{\rm w}$ over which the perturbation acts, so the response grows (going from right to left in Fig. 5(b)). The gradient $\partial\chi/\partial t_{\rm w}$ has an interpretation as the response of the system to an instantaneous (impulse) perturbation applied at $t_{\rm w}$. The only difficulty when obtaining data with fixed t and variable $t_{\rm w}$ is that each value of $t_{\rm w}$ requires a separate computer simulation because the time at which the perturbation is applied is different in each case.

In Fig. 6, we summarise the data of Fig. 5 by making a parametric plot of the response $\tilde{\chi}(t,t_{\rm w})$ as a function of the correlation $\tilde{C}(t,t_{\rm w})$, keeping fixed $t=4000$ MC steps and varying $t_{\rm w}$ and the bond strength. Such fluctuation-dissipation (FD) plots are often used in the study of glassy systems[45,50,54,55]. The bottom right corner, where the correlation is maximum and the response zero, corresponds to $t=t_w$. Following the curves from right to left (decreasing $\tilde{C}(t,t_{\rm w})$), the points indicate the behaviour as $t_{\rm w}$ decreases. The dashed line is the equilibrium FDT, $\tilde{\chi}_{\rm eqm}(t,t_w)=1-\tilde{C}_{\rm eqm}(t,t_w)$. The data for the high temperature system lie on the FDT line, as expected since the system is equilibrated. On crossing the binodal, the bond strength is sufficient to drive phase separation and assembly. In this regime, the data lie on the FDT line when $t-t_{\rm w}$ is small, before deviating as $t-t_{\rm w}$ grows (and $\tilde{C}(t,t_{\rm w})$ shrinks): see for

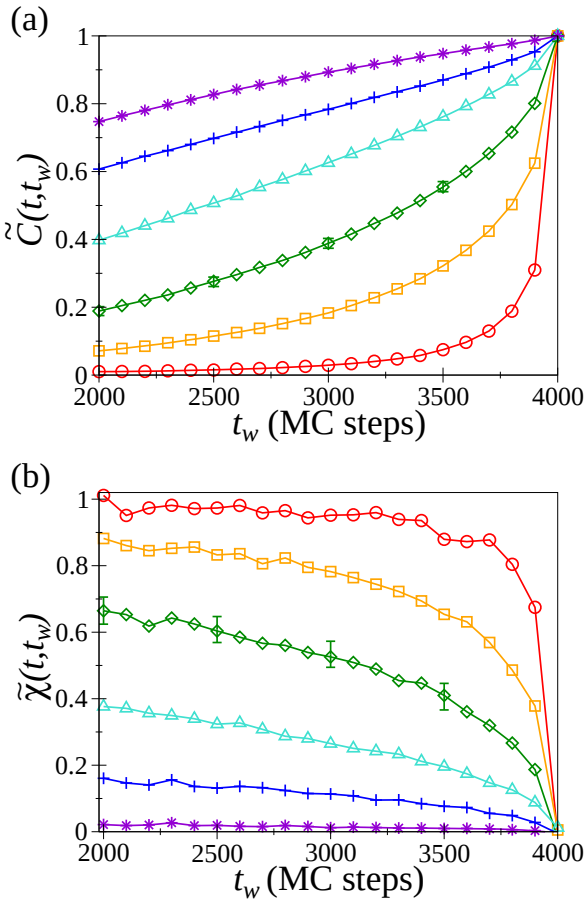

Fig. 5 (a) Correlation $\tilde{C}(t,t_{\rm w})$ plotted against $t_{\rm w}$ for different bond strengths at fixed $t = 4000$. (The symbols for the characteristic bond strengths plotted here were defined in Fig. 1(a) and are also shown in the legend of Fig. 6). (b) Response function $\tilde{\chi}(t,t_{\rm w})$. Correlation and response functions are estimated by averaging over many independent trajectories, with error bars shown for a few representative points in each panel.

example $u = 2.3, 2.6, 3.3$. The time window over which the data lie close to the FDT line decreases as the bonds become stronger, and the low temperature data, $u = 4.5, 7.0$, deviate from the FDT line even when $t - t_{\rm w}$ is very small.

Jack *et al.*[30], argued that if the data are close to the FDT line when $t - t_{\rm w} \approx \tau$, then the behaviour of the system is 'locally equilibrated'[§] on the time scale τ. In this case, the idea is that the region of configuration space explored on these time scales is being explored reversibly. That is, given a movie of the system of length τ and a similar movie where time has been reversed, it would be difficult to discern which is which. Clearly, if this property holds, then the likelihoods of bond-making and bond-breaking must be similar. On long time scales (large $t - t_{\rm w}$), it will be apparent if a system is assembling and bond-making dominates. But if the system is avoiding kinetic traps by exploiting the reversibility of the bonding process in order to anneal out defects[42] then one expects the system to be locally equilibrated over a time interval τ that is comparable to the bond lifetime, and hence that the data in Fig. 6 remain close to the FDT line over a significant range of $\tilde{C}$. As in Ref.[30], this expectation seems to be borne out by these numerical simulations.

Furthermore, as discussed in section 4.1, the response function $\tilde{\chi}(t,t_{\rm w})$ that we use is particularly sensitive to bond-breaking processes. Deviations from reversibility and local equilibrium can be of different types, but it is the balance of bond-making and bond-breaking that is most relevant for annealing and hence assembly. In general, FD measurements may depend strongly on the observable (or perturbation) used[50,55,57,58] – in contrast to our results here, we expect that an analysis of the response to a spatially-dependent perturbation following Russo and Sciortino[50] would lead to an FD plot that is consistent with local equilibrium behaviour even when kinetic trapping is frustrating assembly. Thus, while the specific response we consider may not be directly accessible in experiments, we believe that responses that couple strongly to local annealing processes are required to detect the deviations from local equilibrium that are responsible for kinetic trapping.

4.3 Robustness of results

Comparing Figs. 1 and 6, long-time measurements of the yield are correlated with short-time measurements of correlation and response functions. We have in mind that the short-time measurements might be used to predict the long-time behaviour. However, these systems are far-from-equilibrium, and both the short- and long-time measurements will depend

§ Our use of the term 'local equilibration' is similar in spirit to an analogous condition in non-equilibrium thermodynamics[56], but here we are referring to locality in a region of configuration space, and not in a spatially localised region of the system.

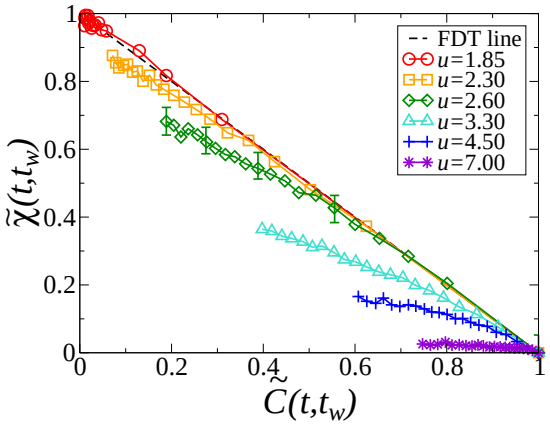

Fig. 6 Parametric plot of $\tilde{\chi}(t,t_{\rm w})$ versus $\tilde{C}(t,t_{\rm w})$. The data are plotted for fixed t=4000 MC steps, varying $t_{\rm w}$ between 2000-4000 MC steps, in steps of 100. The dashed line is $\tilde{\chi}(t,t_w)$=1-$\tilde{C}(t,t_w)$, which is the FDT behaviour at equilibrium. Deviation of the data from the FDT line indicate deviations from local equilibration (see main text).

on the times at which these measurements are made. If the short-time measurements are to be a useful predictive tool, the correlation between short-time and long-time behaviour must be robust to variations in the time at which the measurements are made, as well as to changes in the system parameters (for example, volume fraction and interaction range).

In Fig. 7, we show the effect of varying the measurement times, keeping system parameters constant. Fig. 7(a) shows that measuring the yield at different times leads to differences in the crystallinity of the sample, as expected since the phase transformation is taking place over the whole time window considered. Nevertheless, a change of two orders of magnitude in the measurement time leads to the same qualitative results, and the condition that assembly is optimal for $u \approx 2.5$ is robust. In Fig. 7(b), we show that increasing the time at which the correlation and response measurements are made leads to very small changes in the FD plot. (We show results for the near-optimal condition $u = 2.6$ but the weak dependence on t is similar for other bond strengths.) This insensitivity to changes in t and $t_{\rm w}$ reinforces the idea that the FD plot has potential as a predictive tool, since one arrives at the same prediction, regardless of the specific time at which the measurements are made.

We now discuss dependence on the volume fraction ϕ and the interaction range ξ. Results are summarised in Fig. 8. On increasing the volume fraction from 4% to 16%, the yield (crystallinity at long times) varies only slightly. Increasing ϕ at constant u increases the supersaturation and hence speeds up nucleation, but this effect is rather weak in this system, for

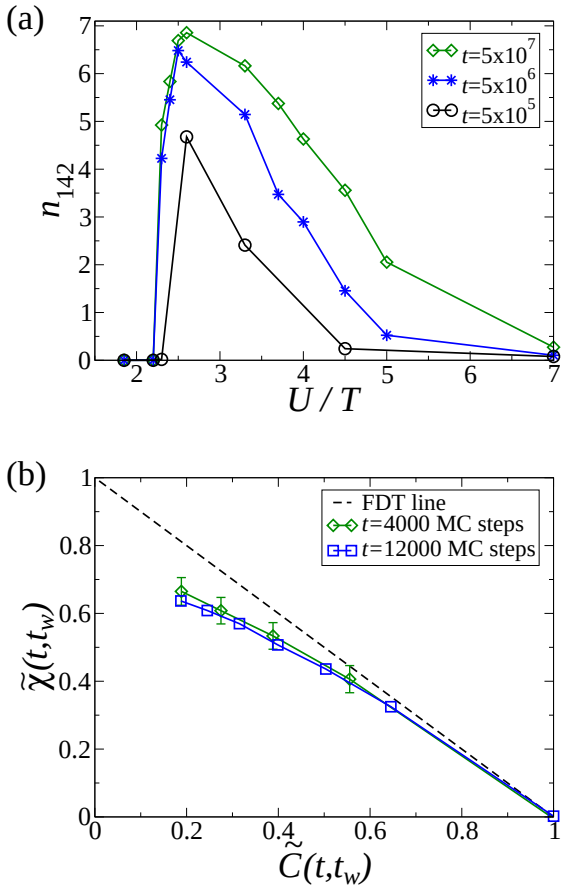

Fig. 7 (a) Yield at various times, plotted as a function of the bond strength (compare Fig. 1(a)). (b) Parametric plot of $\tilde{\chi}(t,t_{\rm w})$ versus $\tilde{C}(t,t_{\rm w})$ for different measurement times: $t = 4000$ MC steps and $2000 < t_{\rm w} < 4000$ MC steps as in Fig. 6 and $t = 12000$ MC steps with $6000 < t_{\rm w} < 12000$ MC steps. The dashed line is $\tilde{\chi}(t,t_w)$=1-$\tilde{C}(t,t_w)$, which is the FDT result at equilibrium.

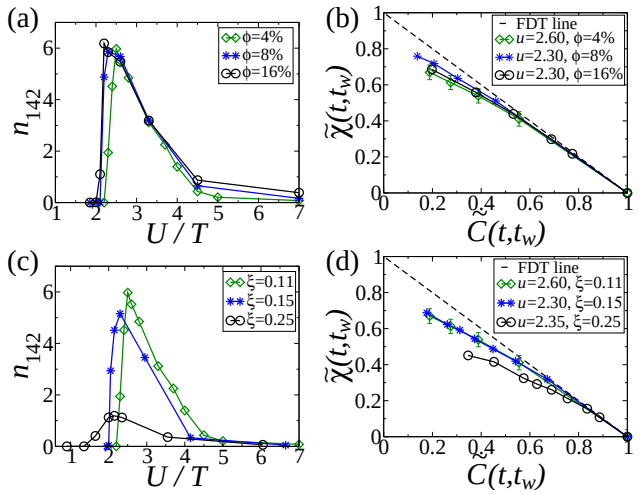

Fig. 8 (a) Measurement of the yield at $t = 10^6$ MC steps, as a function of the bond strength, for three different volume fractions. (b) FD plot, calculated at optimal assembly $u = 2.6$, for three different volume fractions. (c) Yield measurements for three different interaction ranges. (d) FD plot, calculated using the optimal value of u associated with each value of ξ.

these times. In the kinetic-trapping regime, the dependence of the results on volume fraction are surprisingly weak: this is presumably related to the thermally-activated time scales for bond-breaking, which are independent of ϕ. Turning to the correlation-response measurements in 8(b), the dependence on volume fraction is again weak, providing further evidence that FD plots can be used to predict conditions for effective crystallisation.

On increasing the range of the attractive interactions, the phase diagram of the system changes as the liquid phase becomes more stable. For the case $\xi = 0.25$, the fluid-fluid and crystal-fluid binodals are very close to each other (both are near to $u = 1.5$ for $\phi = 4\%$[28]). Changing ξ from 0.11 to 0.25 has a significant effect on the yield (crystallinity) of the self-assembly process. In particular, for $\xi = 0.25$ and a fixed time $t = 10^6$ MC sweeps, the system tends to form amorphous clusters and Fig. 8(c) shows that the yield is rather small for all u. We find that on increasing the measurement time, crystallisation continues to take place and the yield increases significantly. However, the bond strength at maximal yield remains stable at $u \approx 2$ (data not shown). In Fig. 8(d), we show FD plots for various ξ, where the value of u is chosen in each case to be near-optimal for the long-time yield. Quantitative differences are apparent as ξ is varied, but we believe that the FD plots at optimal assembly are similar enough for predictions of effective crystallisation conditions to be made.

5 Outlook

We have considered how we might predict the evolution of a model colloidal system based on the dynamics at early times, as presented schematically in Fig. 3(a). The parametric plot in Fig. 6 provides a measurement that has a characteristic form when self-assembly (crystallisation) is effective. In this regime, the response $\tilde{\chi}(t,t_w)$ is close to its FDT prediction $1-\tilde{C}(t,t_w)$ when $t-t_w$ is small, with significant deviations appearing as $t-t_w$ increases. The kinetic trapping regime is characterised by much smaller values of $\tilde{\chi}(t,t_w)$. On the other hand, the regime where weak bonds lead to poor assembly is characterised by data that are very close to the FDT prediction for a wide range of $t-t_w$. We emphasise that these measurements are made before any structural signature of crystallisation is apparent in our samples: instead, the correlation and response functions provide a quantitative measure of the reversibility of bond formation[42–44] through the time scale τ discussed in section 4.2.

The current paper complements a previous study[30], indicating that the method is applicable at least to patchy particles that form viral capsids, as well as to discs and spheres with short-ranged attractive interactions. These systems have diverse kinetically trapped states and may have no equilibrium phase transitions at all (viral capsids), or phase transitions to both stable crystalline and metastable liquid states (as in this work). Despite these differences, the correlations between parametric plots such as Fig. 6 and yield measurements such as Fig. 1(b) seem to be conserved between models, indicating that the method may have broad application. We also note that parametric FD plots are 'dimensionless' in that they may be directly compared between different systems: the only free parameter associated with this comparison is the time t associated with the parametric plot. We showed in Fig. 7(a) that results for this crystallising system depend weakly on this time, strengthening the argument that comparison of plots from different systems under different conditions can be compared fairly with each other. In the future, we hope that the predictive information in such measurements might be useful in optimising computer simulations of assembling systems, and perhaps even experimental crystallisation and self-assembly processes.

Acknowledgments

We thank Mike Hagan, Paddy Royall, Steve Whitelam, and David Chandler for many useful discussions. This work was supported by the EPSRC through grants EP/G038074/1 and EP/I003797/1.

A Calculation of response function

This section explains how the response function in Eq.(6) is calculated in simulations. For compactness of notation, we write $h_i = \delta U_i/2T$ so the response of Eq.(6) is

$$\chi(t,t_{\rm w}) = \frac{1}{4}\frac{\partial\langle n_i(t)\rangle}{\partial h_i} \tag{A.1}$$

where the field is applied between times t and $t_{\rm w}$. We run simulations where h_i is finite for all particles: we take $h_i = |h|$ for half of the particles (chosen at random), with $h_i = -|h|$ for the other half.

In the presence of such a perturbation, we make a Taylor expansion of $\langle n_i\rangle_h$, where the subscript h indicates the presence of the N perturbing fields $h_1,\ldots,h_N$. The result is

$$\langle n_i\rangle_h = \langle n_i\rangle + h_i\frac{\partial\langle n_i\rangle}{\partial h_i} + \sum_{j\neq i} h_j\frac{\partial\langle n_i\rangle}{\partial h_j} + O(h^2) \tag{A.2}$$

where all derivatives are evaluated at $h = 0$ and we omit the dependence of n_i on time t, for brevity. The first-order terms in the Taylor expansion are the response of particle i to its own field h_i, and the response of this particle to the specific combination of other fields.

For $j \neq i$, the response $\frac{\partial\langle n_i\rangle}{\partial h_j}$ is independent of i and j, and scales as N^{-1} in the thermodynamic limit. We therefore write, for $i \neq j$,

$$\frac{\partial\langle n_i\rangle}{\partial h_j} = \frac{c}{N} \tag{A.3}$$

with $c = O(1)$ as $N \to \infty$ (see below).

We now decompose the sum over j in (A.2) into a contribution from those particles j for which $h_j > 0$, and those with $h_j < 0$. Restricting to $j \neq i$, let S_+ be the set of particles j for which $h_j > 0$ and S_- the set with $h_j < 0$. In (A.2), all terms in the sum are equal to either $+|h|c/N$ or $-|h|c/N$, so if the number of particles in S_+ is N_+ and the number in S_- is N_- then we have

$$\sum_{j\neq i} h_j\frac{\partial\langle n_i\rangle}{\partial h_j} = (N_+ - N_-)\frac{|h|c}{N}. \tag{A.4}$$

and hence

$$\langle n_i\rangle_h = \langle n_i\rangle + h_i\frac{\partial\langle n_i\rangle}{\partial h_i} + |h|c\frac{N_+ - N_-}{N} + O(h^2) \tag{A.5}$$

It is clear from this equation that we require $c = O(1)$ as $N \to \infty$ (see above) so that the response is finite if (for example) a positive field is applied to exactly half of the particles and the other particles are unchanged ($N_+ = \frac{N}{2}$ and $N_- = 0$).

In the case where half of the particles receive a perturbation of $+|h|$ and half receive $-|h|$, the value of $\langle n_i\rangle_h$ depends on i only through the sign of h_i. For particles with $h_i > 0$, we write their average number of neighbours by $\langle n_i\rangle_+$ while for particles with $h_i < 0$ we write $\langle n_i\rangle_-$. These quantities are readily calculated in a simulation, by evaluating the number of bonds for each particle and averaging separately over those with $h_i > 0$ and those with $h_i < 0$.

In total, $\frac{N}{2}$ particles have $h_i > 0$ and $\frac{N}{2}$ have $h_i < 0$. However, the sets S_+ and S_- both exclude particle i, so if $h_i > 0$ then $N_+ = \frac{N}{2} - 1$ while $N_- = \frac{N}{2}$. Hence

$$\langle n_i\rangle_+ = \langle n_i\rangle + |h|\frac{\partial\langle n_i\rangle}{\partial h_i} - |h|\frac{c}{N} + O(h^2) \tag{A.6}$$

Similarly if $h_i < 0$, then $N_+ = \frac{N}{2}$ while $N_- = \frac{N}{2} - 1$, so that

$$\langle n_i\rangle_- = \langle n_i\rangle - |h|\frac{\partial\langle n_i\rangle}{\partial h_i} + |h|\frac{c}{N} + O(h^2) \tag{A.7}$$

It is therefore clear that the average particle energy in the absence of the field may be estimated in the perturbed system by

$$\langle n_i\rangle = \frac{\langle n_i\rangle_+ + \langle n_i\rangle_-}{2} + O(h^2) \tag{A.8}$$

while the single particle response function can be estimated as

$$\frac{\partial\langle n_i\rangle}{\partial h_i} = \frac{\langle n_i\rangle_+ - \langle n_i\rangle_-}{2|h|} + O(|h|) + O(1/N) \tag{A.9}$$

That is, the response $\chi(t,t_{\rm w})$ in Eqs.(6) and (A.1) can be estimated as $\chi(t,t_{\rm w}) = \frac{T}{4|\delta U|}(\langle n_i\rangle_+ - \langle n_i\rangle_-)$ by measuring the difference in the number of neighbours of particles for which the perturbing field δU_i has positive or negative sign. This is the method used to calculate $\chi(t,t_{\rm w})$ in this article.

B Fluctuation-dissipation theorem

In this section, we prove Eq.(8) of the main text. As in the previous section, we write $h_i = \delta U_i/2T$. The response of Eq.(6) may be written in terms of probabilities by using (A.1) together with

$$\frac{\partial\langle n_i\rangle}{\partial h_i} = \frac{\partial}{\partial h_i}\left(\sum_{I,F}\rho(I)G^h_{t-t_{\rm w}}(I\to F)n_i(F)\right), \tag{B.1}$$

where I is the configuration of the system at time $t_{\rm w}$ and F is the configuration at time t: the sum runs over all possible configurations I and F. Also, $n_i(F)$ is the number of neighbours of particle i in configuration F; the initial distribution $\rho(I)$ is the probability of being in configuration I at time $t_{\rm w}$; and the propagator $G^h_{t-t_{\rm w}}(I\to F)$ is the probability of being in configuration F at time t, given that the system was in configuration I at time $t_{\rm w}$. The label h on the propagator indicates that it depends on the applied fields h_i, while $\rho(I)$ and $n_i(F)$ do not.

Since we are concerned with Eq.(8), we restrict to the case of equilibrium response functions, for which the system is equilibrated with $h = 0$ at time t_w:

$$\rho(I) = \rho_{\rm eqm}^{h=0}(I) = \frac{{\rm e}^{uB(I)}}{Z}, \tag{B.2}$$

where $Z = \sum_I {\rm e}^{uB(I)}$ and $B(I) = \frac{1}{2}\sum_i n_i(I)$ is the total number of bonds in configuration I. The energy of configuration I in the unperturbed system is $-UB(I)$ while in the perturbed system it is $-UB(I) - T\sum_i h_i n_i(I)$. Hence we define

$$\rho_{\rm eqm}^{h}(I) = \frac{1}{Z_h}{\rm e}^{uB(I)+\sum_i h_i n_i(I)}, \tag{B.3}$$

with $Z_h = \sum_I {\rm e}^{uB(I)+\sum_i h_i n_i(I)}$ the partition function.

To prove Eq.(8) we make use of detailed balance. For a single Monte Carlo step in the presence of the perturbation h, let the probability of arriving in configuration J from an initial configuration I be $P^h(I \to J)$. Detailed balance states that

$$\rho_{\rm eqm}^{h}(I)P^h(I \to J) = \rho_{\rm eqm}^{h}(J)P^h(J \to I), \tag{B.4}$$

which ensures that the system converges to the equilibrium distribution in the limit of long times. A similar relation follows for the propagator:

$$\rho_{\rm eqm}^{h}(I)G_{t-t_w}^h(I \to F) = \rho_{\rm eqm}^{h}(F)G_{t-t_w}^h(F \to I). \tag{B.5}$$

In (B.1), the only h-dependence comes through G^h so we seek an expression for $\frac{\partial}{\partial h_i}G^h$. We use detailed balance together with (B.3) to write

$$G_{t-t_w}^h(I \to F) = G_{t-t_w}^h(F \to I)\times {\rm e}^{uB(F)-uB(I)+\sum_i[h_i n_i(F)-h_i n_i(I)]}. \tag{B.6}$$

Taking a derivative with respect to h_i and evaluating it at $h = 0$, we arrive at

$$\frac{\partial}{\partial h_i}G_{t-t_w}^h(I \to F) = {\rm e}^{uB(F)-uB(I)}\times \left[(n_i(F) - n_i(I))G_{t-t_w}^{h=0}(F \to I) + \frac{\partial}{\partial h_i}G_{t-t_w}^h(F \to I)\right]. \tag{B.7}$$

Now, detailed balance implies that ${\rm e}^{uB(F)-uB(I)}G_{t-t_w}^{h=0}(F \to I) = G_{t-t_w}^{h=0}(I \to F)$, and we also have $\rho_{\rm eqm}^{h=0}(F){\rm e}^{uB(I)-uB(F)} = \rho_{\rm eqm}^{h=0}(I)$. Combining these results with (B.1) and (B.7) yields

$$\frac{\partial\langle n_i\rangle}{\partial h_i} = \sum_{I,F}\rho_{\rm eqm}^{h=0}(I)G_{t-t_w}^{h=0}(I \to F)[n_i(F) - n_i(I)]n_i(F) + \sum_{I,F}\rho_{\rm eqm}^{h=0}(F)\frac{\partial}{\partial h_i}G_{t-t_w}^h(F \to I)n_i(F), \tag{B.8}$$

where we recognise the first term on the right hand side as the correlation function $\langle n_i(t)[n_i(t) - n_i(t_w)]\rangle$, evaluated at equilibrium. The second term on the right hand side is zero since $\sum_I G_{t-t_w}^h(F \to I) = 1$: this follows from the definition of $G_{t-t_w}(F \to I)$ as the probability of being in state I at time t since these probabilities must sum to unity, regardless of F, h and $t - t_w$.

Hence, at equilibrium, (B.8) reduces to

$$\frac{\partial\langle n_i\rangle}{\partial h_i} = \langle n_i(t)[n_i(t) - n_i(t_w)]\rangle. \tag{B.9}$$

To recover Eq.(8) of the main text, we note from (4) that

$$C(t,t_w) = \tfrac{1}{4}[\langle n_i(t)n_i(t_w)\rangle - \langle n_i(t)\rangle\langle n_i(t_w)\rangle] \tag{B.10}$$

so that the right hand side of (B.9) is $4[C(t,t) - C(t,t_w)] + \langle n_i(t)\rangle\langle n_i(t) - n_i(t_w)\rangle$. At equilibrium, time-translational invariance implies $\langle n_i(t) - n_i(t_w)\rangle = 0$, and using (A.1) with (B.9) one arrives at the fluctuation-dissipation theorem

$$\chi_{\rm eqm}(t,t_w) = C_{\rm eqm}(t,t) - C_{\rm eqm}(t,t_w). \tag{B.11}$$

Finally, dividing both sides by $C_{\rm eqm}(t,t)$ yields the normalised version of the FDT, which is given in Eq.(8).

References

1 R. Langer and D. A. Tirrel, *Nature*, 2004, **428**, 487–492.
2 S. I. Stupp, *Nano Lett.*, 2010, **10**, 4783.
3 J. C. Love, L. A. Estroff, J. K. Kriebel, R. G. Nuzzo and G. M. Whitesides, *Chem. Rev.*, 2005, **105**, 1103–1169.
4 M. Mastrangeli, S. Abbasi, C. Varel, C. V. Hoof, J.-P. Celis and K. F. Bohringer, *J. Micromech. Microeng.*, 2009, **1**, 083001.
5 G. M. Whitesides and D. J. Lipomi, *Faraday Discuss.*, 2009, **143**, 373–384.
6 S. Srivastava, A. Santos, K. Critchley, K.-S. Kim, P. Podsiadlo, K. Sun, J. Lee, C. Xu, G. D. Lilly, S. C. Glotzer and N. A. Kotov, *Science*, 2010, **327**, 1355.
7 Y. Wang and W. Zhou, *J. Nanosci. Nanotech.*, 2010, **10**, 1563–1583.
8 M. Grzelczak, J. Vermant, E. M. Furst and L. M. Liz-Marzan, *ACS Nano*, 2010, **4**, 3591–3605.
9 S. C. Glotzer and M. J. Solomon, *Nature Materials*, 2007, **6**, 557–562.
10 L. Hong, A. Cacciuto, E. Luijten and S. Granick, *Nano Lett.*, 2006, **6**, 2510–2514.
11 S. M. Douglas, H. Dietz, T. Liedl, B. Hogberg, F. Graf and W. M. Shih, *Nature*, 2009, **459**, 414–418.
12 S. Sacanna, W. T. M. Irvine, P. M. Chaikin and D. J. Pine, *Nature*, 2010, **464**, 575–578.
13 A. Bray, *Adv Phys*, 1994, **43**, 357–459.
14 L. Slabinski, L. Jaroszewski, A. P. C. Rodrigues, L. Rychlewski, I. A. Wilson, S. A. Lesley and A. Godzik, *Protein Sci.*, 2007, **16**, 2472–2482.
15 J. Leng and J.-B. Salmon, *Lab Chip*, 2009, **9**, 24–34.
16 P. J. Lu, J. C. Conrad, H. M. Wyss, A. B. Schofield and D. A. Weitz, *Phys. Rev. Lett.*, 2006, **96**, 028306.
17 S. Whitelam, E. H. Feng, M. F. Hagan and P. L. Geissler, *Soft Matter*, 2009, **5**, 1251–1262.
18 N. E. Chayen, *Curr. Opinion Struct. Biol.*, 2004, **14**, 577 – 583.

19 Y. A. Vlasov, X.-Z. Bo, J. C. Sturm and D. J. Norris, *Nature*, 2001, **414**, 289–293.
20 A.-P. Hynninen, J. H. J. Thijssen, E. C. M. Vermolen, M. Dijkstra and A. Van Blaaderen, *Nature Mat.*, 2007, **6**, 202–205.
21 P. ten Wolde and D. Frenkel, *Science*, 1997, **277**, 1975–1978.
22 C. N. Likos, *Phys. Rep.*, 2001, **348**, 267–439.
23 G. Foffi, G. D. McCullagh, A. Lawlor, E. Zaccarelli and K. A. Dawson, *Phys. Rev. E*, 2002, **65**, 031407.
24 M. Dijkstra, *Phys. Rev. E*, 2002, **66**, 021402.
25 F. W. Tavares and J. M. Prausnitz, *Colloid Polym. Sci.*, 2004, **282**, 620.
26 P. Charbonneau and D. R. Reichman, *Phys. Rev. E*, 2007, **75**, 011507.
27 A. Fortini, E. Sanz and M. Dijkstra, *Phys. Rev. E*, 2008, **78**, 041402.
28 H. Liu, S. Garde and S. Kumar, *J. Chem. Phys.*, 2005, **123**, 174505.
29 J. D. Honeycutt and H. C. Andersen, *J. Phys. Chem.*, 1987, **91**, 4950–4963.
30 R. L. Jack, M. F. Hagan and D. Chandler, *Phys. Rev. E*, 2007, **76**, 021119.
31 S. Whitelam, *arXiv:1009.2008v2 [cond-mat.stat-mech]*, 2011.
32 R. T. Scarlett, J. C. Crocker and T. Sinno, *J. Chem. Phys.*, 2010, **132**, 234705.
33 A. Chatterjee and D. Vlachos, *J. Comp.-Aided Mat. Des.*, 2007, **14**, 253.
34 A. F. Voter, *Phys. Rev. B*, 1986, **34**, 6819.
35 S. Auer and D. Frenkel, *J Chem Phys*, 2004, **120**, 3015–3029.
36 R. P. Sear, *J. Phys.: Condens. Matter*, 2007, **19**, 033101.
37 S. R. Williams, C. P. Royall and G. Bryant, *Phys. Rev. Lett.*, 2008, **100**, 225502.
38 L. Filion, M. Hermes, R. Ni and M. Dijkstra, *J. Chem. Phys.*, 2010, **133**, 244115.
39 S. Whitelam, *Phys. Rev. Lett.*, 2010, **105**, 088102.
40 T. Schilling, H. J. Schöpe, M. Oettel, G. Opletal and I. Snook, *Phys. Rev. Lett.*, 2010, **105**, 025701.
41 W. Lechner, C. Dellago and P. G. Bolhuis, *Phys. Rev. Lett.*, 2011, **106**, 085701.
42 G. M. Whitesides and M. Boncheva, *Proc. Natl. Acad. Sci. U. S. A.*, 2002, **99**, 4769.
43 M. Hagan and D. Chandler, *Biophys. J.*, 2006, **91**, 42–54.
44 D. C. Rapaport, *Phys. Rev. Lett.*, 2008, **101**, 186101.
45 L. F. Cugliandolo, J. Kurchan and L. Peliti, *Phys. Rev. E*, 1997, **55**, 3898–3914.
46 A. Crisanti and F. Ritort, *J. Phys. A: Math. Gen.*, 2003, **36**, R181–R290.
47 J. Kurchan, *Nature*, 2005, **433**, 222–225.
48 M. Baiesi, C. Maes and B. Wynants, *Phys. Rev. Lett.*, 2009, **103**, 010602.
49 U. Seifert and T. Speck, *EPL*, 2010, **89**, 10007.
50 J. Russo and F. Sciortino, *Phys. Rev. Lett.*, 2010, **104**, 195701.
51 S. Jabbari-Farouji, D. Mizuno, M. Atakhorrami, F. C. MacKintosh, E. E. Christoph F. Schmidt, G. H. Wegdam and D. Bonn, *Phys. Rev. Lett.*, 2007, **98**, 108302.
52 C. Maggi, R. D. Leonardo, J. C. Dyre and G. Ruocco, *Phys. Rev. B*, 2010, **81**, 104201.
53 H. Oukris and N. E. Israeloff, *Nature Physics*, 2010, **6**, 135–138.
54 P. Sollich, S. Fielding and P. Mayer, *J. Phys. Condens. Matter*, 2002, **14**, 1683.
55 R. L. Jack, L. Berthier and J. P. Garrahan, *J. Stat. Mech.*, 2006, P12005.
56 S. de Groot and P. Mazur, *Non-equilibrium thermodynamics*, Dover, Mineola NY, 1984.
57 S. Fielding and P. Sollich, *Phys. Rev. Lett.*, 2002, **88**, 050603.
58 G. Diezemann and R. Bohmer, *J. Chem. Phys.*, 2006, **124**, 214507.